Coexistence of Strong and Weak Topological Orders in a Quasi-One-Dimensional Material

De-Yang Wang,[1,2] Qi Jiang,[1,2] Kenta Kuroda,[3,*] Kaishu Kawaguchi,[3] Ayumi Harasawa,[3] Koichiro Yaji,[4] Arthur Ernst,[5,6] Hao-Ji Qian,[1,2] Wen-Jing Liu,[1,2] He-Ming Zha,[1,2] Zhi-Cheng Jiang,[1,2] Ni Ma,[1,2] Hong-Ping Mei,[1,2] Ang Li,[1,2] Takeshi Kondo,[3,7,†] Shan Qiao,[1,2,8,‡] and Mao Ye[1,2,‖]

[1]*State Key Laboratory of Functional Materials for Informatics, Shanghai Institute of Microsystem and Information Technology, Chinese Academy of Sciences, Shanghai 200050, People's Republic of China*

[2]*Center of Materials Science and Optoelectronics Engineering, University of Chinese Academy of Sciences, Beijing 100049, People's Republic of China*

[3]*Institute for Solid State Physics, The University of Tokyo, Kashiwa, Chiba 277-8581, Japan*

[4]*Research Center for Advanced Measurement and Characterization, National Institute for Materials Science, Ibaraki 305-0003, Japan*

[5]*Institute for Theoretical Physics, Johannes Keppler University Linz, Altenberger Strasse 69, A-4040 Linz, Austria*

[6]*Max-Planck-Institut fur Mikrostrukturphysik, Weinberg 2, D-06120 Halle, Germany*

[7]*Trans-scale Quantum Science Institute, The University of Tokyo, Bunkyo-ku, Tokyo 113-0033, Japan*

[8]*School of Physical Science and Technology, ShanghaiTech University, Shanghai 201210, People's Republic of China*

(Received 18 November 2021; revised 12 July 2022; accepted 12 August 2022; published 28 September 2022)

Topological materials have broad application prospects in quantum computing and spintronic devices. Among them, dual topological materials with low dimensionality provide an excellent platform for manipulating various topological states and generating highly conductive spin currents. However, direct observation of their topological surface states still lacks. Here, we reveal the coexistence of the strong and weak topological phases in a quasi-one-dimensional material, $TaNiTe_5$, by spin- and angle- resolved photoemission spectroscopy. The surface states protected by weak topological order forms Dirac-node arcs in the vicinity of the Fermi energy, providing the opportunity to develop spintronics devices with high carrier density that is tunable by bias voltage.

DOI: 10.1103/PhysRevLett.129.146401

The discovery of topological materials has drawn widespread attention in the field of condensed matter physics in recent decades [1,2]. Because of the protection of space and time inversion symmetry, topological materials possess nontrivial edge states with high conductivity, where the backscattering is strictly prohibited. Such a feature protects electrons from suffering perturbation of nonmagnetic impurities. Therefore, topological materials provide a broad platform for the further development of quantum physics, such as realizing Majorana zero modes [3] and the quantum anomalous Hall effect [4].

Topological materials are mainly classified into several categories through topological index: strong topological materials [5], weak topological materials [5], topological crystalline materials [6], and higher-order topological materials [7]. Whereas these topological orders in certain material are not exclusive [8], topological states originated from different categories may coexist in one material simultaneously. Materials with multiple topological phases not only enable distinct crystal planes to achieve specific functions, but also have great potential to regulate a variety of topological transitions independently by breaking particular symmetry, such as applying external strain or magnetic fields.

For a long time, dual topological materials have only existed in theoretical conceptions, while only a few have been experimentally realized. In recent work, Bi_2TeI was verified as a dual topological material via scanning tunneling microscopy (STM) combined with density functional theory (DFT) calculations [9,10]. The analysis of scanning tunneling spectroscopy (STS) and quasiparticle interference (QPI) conclude that the metallic surface states are derived from the topological crystalline order [10]. Meanwhile, the conductive channels residing at the Bi_2-layer edges that originate from the weak topological order have been successfully detected by STS measurements [10]. However, since the weak topological state only exists at specific surfaces of materials, such as the side-surface perpendicular to the van der Waals (vdW) layer in the case of Bi_2TeI, the direct visualization of the weak topological state in the momentum space is still challenging.

On the other hand, the Bi_2-layer structure with hexagonal lattice in Bi_2TeI materials leads to six equivalent edges, suggesting that the weak topological states are distributed in different directions and might interfere with each other. For quasi-one-dimensional (1D) materials, backscattering will be even more strictly prohibited due to the anisotropic 1D conductive channels that facilitate the generation of highly directional spin current and benefit the development of spintronics devices with low energy consumption [11,12]. The family $TaXTe_5$ (X = Ni, Pd, Pt) [13–15] was recently

 © 2022 American Physical Society

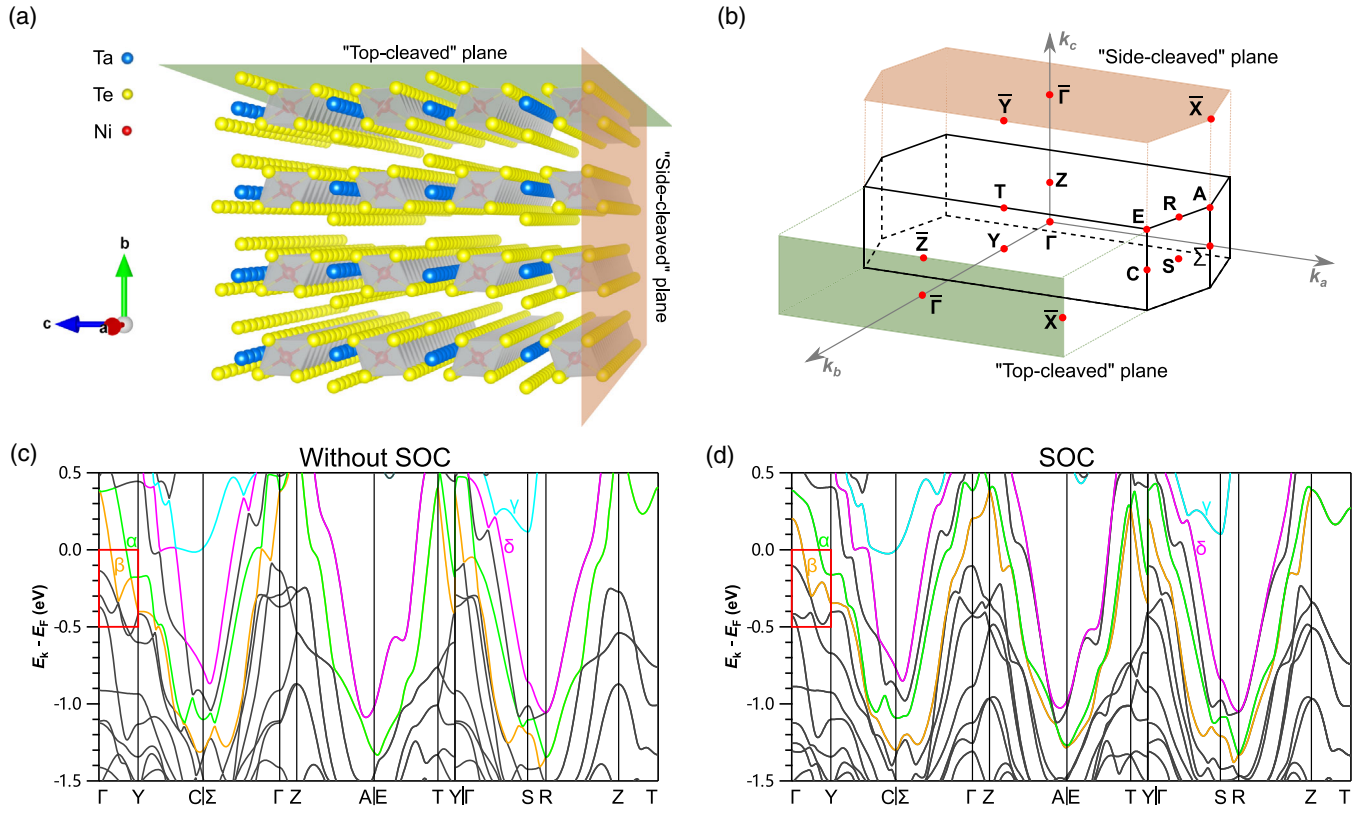

FIG. 1. Crystal structure and calculated bulk bands of $TaNiTe_5$: (a) Crystal structure of $TaNiTe_5$ with its two cleaved planes, indicated by different colors. (b) Bulk Brillouin zone (BZ) and projected surface BZ for the two cleaved planes. (c),(d) Calculated band structures without and with SOC. The band inversion around the Y point between α and β is indicated by red rectangles.

predicted to be candidates for quasi-1D topological materials that possess stable chemical properties. Highly anisotropic transport properties and nontrivial Berry phases have already been confirmed experimentally in TaXTe$_5$ [13–15] together with several intriguing properties in their electronic structures, such as ferroelectriclike polarization [16] and nodal lines [17,18]. Although these materials have similar crystal structures and transport characteristics, their topological classifications obtained from theoretical calculations are diametrically diverse: $TaNiTe_5$ and $TaPdTe_5$ are predicted to be in the strong topological category [13,14] while $TaPtTe_5$ belongs to the weak category [15]. Different theoretical results of topological properties for this family imply that TaXTe$_5$ might be an ideal carrier of multiple topological orders. Hence, to comprehensively investigate topological properties of TaXTe$_5$ is of vital significance for further research.

In this Letter, we unambiguously reveal the coexistence of strong and weak topological orders in quasi-1D $TaNiTe_5$ crystal through high-resolution ARPES and spin-resolved ARPES (SARPES) combined with DFT calculations. We experimentally confirmed the gap opening in the bulk electronic states arising from spin-orbital coupling (SOC), leading to the occurrence of band inversion, as supported by our DFT calculations. ARPES experiments reveal that there are topological surface states in the gap on the "side-cleaved" surface, and their projections on the plane of the vdW layers was proved to possess Dirac-like spin polarizations by laser-based SARPES, confirming the strong topological order. In addition, the Dirac-node arc surface states were observed on the side-cleaved surface near the Fermi energy and proved to be a weak topological phase by DFT calculations, suggesting that they should be responsible for the strong anisotropy in the transport measurements [13]. These results prove $TaNiTe_5$ as a prototype material with great significance to explore novel low-dimensional quantum phenomena, which facilitate the development of spintronics.

The crystal structure of $TaNiTe_5$ belongs to the orthorhombic space group ($Cmcm$, No. 63) with the following lattice parameters: $a = 3.659(2)$ Å, $b = 13.122(10)$ Å, $c = 15.111(11)$ Å, and $\alpha = \beta = \gamma = 90°$. The $NiTe_2$ quasi-1D atomic chains [Fig. 1(a)] extend along the a direction, whereas the vdW layers stack along the b direction. The two planes with different colors indicate two distinct cleaved planes: the "top-cleaved" plane [(010) plane] is cleaved from the vdW layers and the side-cleaved plane [(001) plane] is cleaved perpendicular to the vdW layers. Their corresponding surface Brillouin zones (BZ)

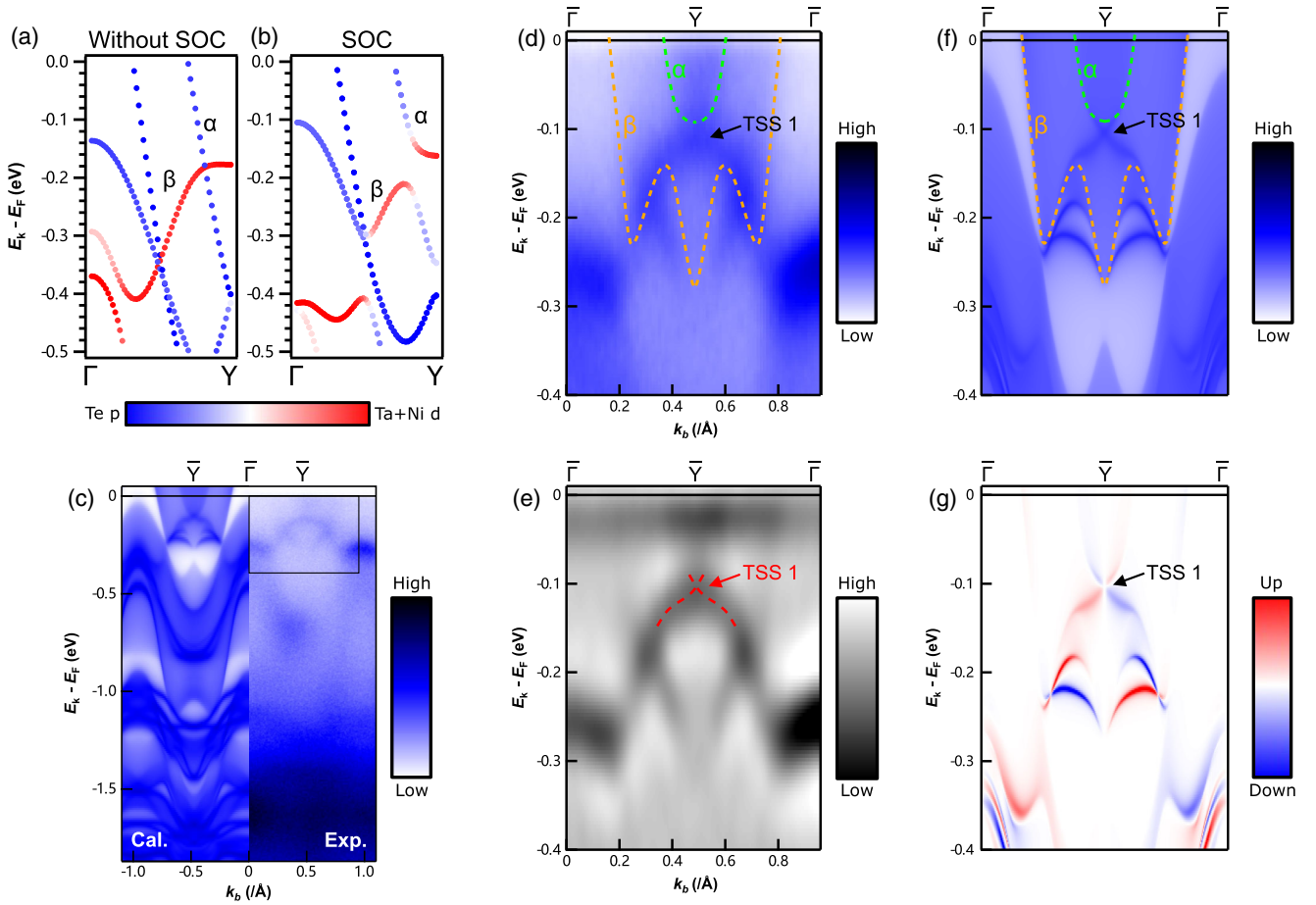

FIG. 2. Band structures for side-cleaved plane of $TaNiTe_5$: (a),(b) Calculated bulk bands along the Γ-Y direction without and with SOC. (c) Calculated (left) and measured (right, $h\nu = 70$ eV, $T_{\text{sample}} = 15$ K) electronic states along the $\bar{\Gamma}$-$\bar{Y}$-$\bar{\Gamma}$ direction, respectively. (d) Magnified view of the area indicated by a black rectangle in (c), showing the TSS1 in the bulk band gap between α and β (plotted by green and yellow dashed lines, respectively). (e) Corresponding 2nd derivative spectrum in the same region of (d), where TSS 1 are guided by red dashed lines. (f) Band dispersions and (g) spin texture obtained from calculations corresponding to (d).

are shown as colored planes in Fig. 1(b) projected from the bulk BZ (black solid lines).

Strong topological order.—First, we performed DFT calculations using the Vienna *ab initio* simulation package [19–21] to examine the topology of the bulk energy bands of $TaNiTe_5$ along high-symmetry directions without and with SOC [Figs. 1(c) and 1(d)], respectively. A clear gap opens between the α band (green) and the β band (yellow) around the Y point along the Γ-Y direction when SOC is included (red rectangle).

To study the topological properties of $TaNiTe_5$ further, we analyze the electron orbital components. The energy bands near the Fermi energy are mainly composed of d orbitals of Ta and Ni, and p orbitals of Te. The band components before and after SOC induced along the Γ-Y direction were compared in Figs. 2(a) and 2(b), showing a gap opening of 40 meV around the Y point after including SOC. At the same time, a band inversion occurs between the d orbitals of Ni/Ta (red) and the p orbitals of Te (blue). This indicates that there is a topologically nontrivial phase in $TaNiTe_5$ near the Y point along the $\bar{\Gamma}$-$\bar{Y}$ direction, corresponding to the side-cleaved plane in real space, at which the presence of topological surface states is expected.

The experimentally measured band structures obtained at the side-cleaved plane are shown in Figs. 2(c)–2(e), visualizing the electronic states along the $\bar{\Gamma}$-$\bar{Y}$ direction in the surface BZ, where the band inversion occurs. Owing to the relatively small beam spot size of the synchrotron light source, ~7.5 (V)μm × 67 (H)μm [22,23], the band dispersion can be clearly observed at the side-cleaved surface. Note that, because the bonding between Te–Te atoms is relatively weak, our calculations for the surface spectrum obtained by the WannierTools package [24,25] in Fig. 2(c) mainly consider the case of Te atom termination, which matches well with ARPES measurements (also see Fig. S2 in the Supplemental Material[26]). The band structures along the high-symmetry direction $\bar{\Gamma}$-$\bar{Y}$-$\bar{\Gamma}$ [Fig. 2(d)] show that, between 0.1 and 0.2 eV below the Fermi energy near the $\bar{Y}$ point, a set of Dirac-type bands (TSS1) has been clearly resolved (indicated by a black

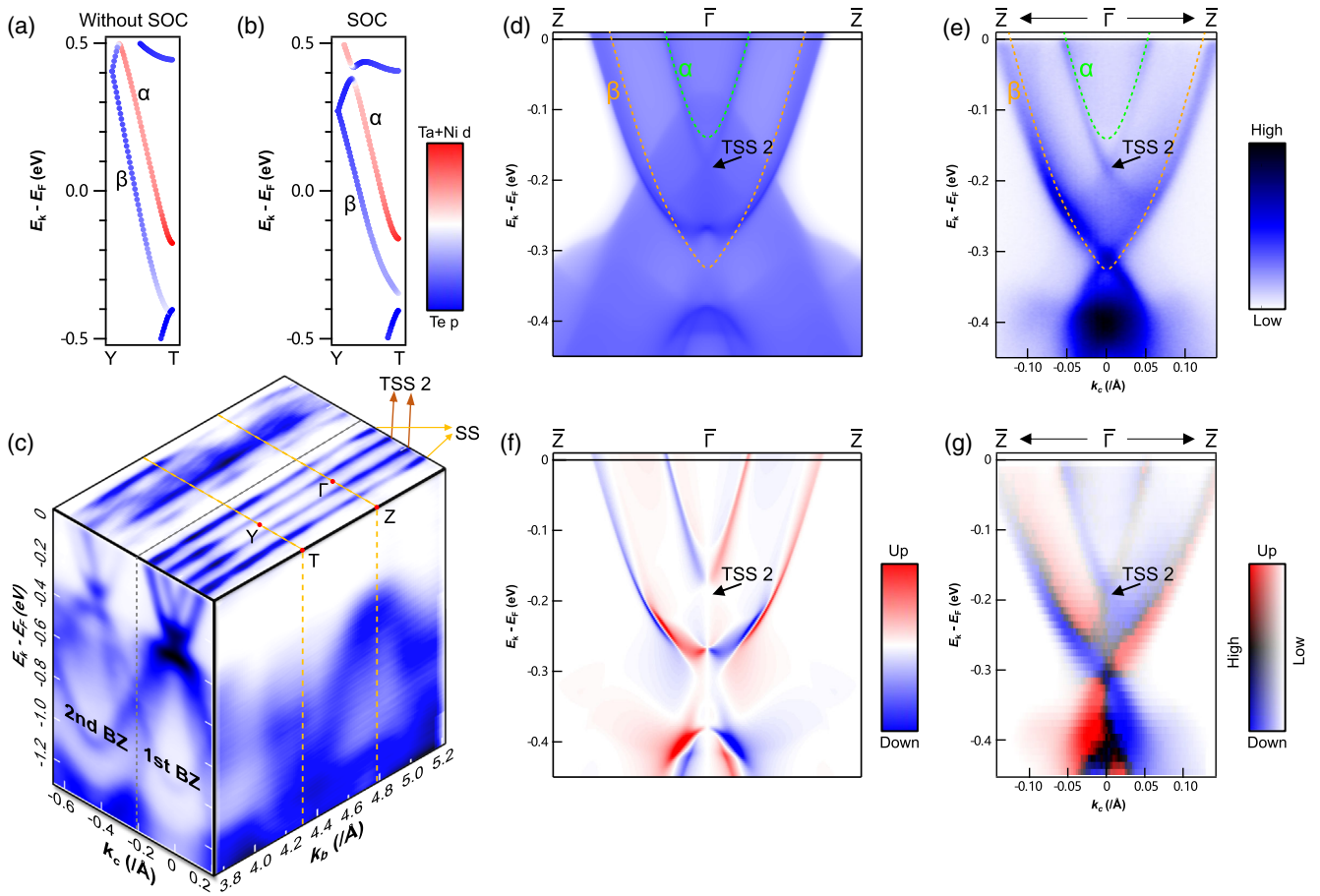

FIG. 3. Band structures for the top-cleaved plane of $TaNiTe_5$: (a),(b) Calculated bulk bands along the T-Y direction without and with SOC. (c) Band structures along $\bar{Z}$-$\bar{\Gamma}$-$\bar{Z}$ direction measured with various photon energy from 50–100 eV (high-symmetry points are marked in red). (d),(f) Calculated band structures and spin texture along the $\bar{Z}$-$\bar{\Gamma}$-$\bar{Z}$ direction (colored lines mark the bulk bands and the black arrow indicates TSS2). (e),(g) Spin-integrated and spin-resolved band structures along the $\bar{Z}$-$\bar{\Gamma}$-$\bar{Z}$ direction obtained in laser-based SARPES measurement.

arrow), which appears clearer on the 2nd derivative spectrum [Fig. 2(e)]. This set of bands crosses the gap where the band inversion occurs and connects α and β bands as our DFT calculations reproduced [Fig. 2(f)]. Note that such Dirac-type bands show nondispersive feature along the k_b direction when it is measured by continuously varied photon energies, evidencing its surface nature of such topological states (see Fig. S4 [26]). Furthermore, the calculated spin texture along the k_b direction [Fig. 2(g)] indicates that the TSS1 are topologically nontrivial electronic states with helical spin texture. This further proves the presence of the topological surface states at the side-cleaved surface of $TaNiTe_5$.

As a material with strong topological phase, Dirac-type surface states should be observed also at other surfaces [5]. Therefore, we examined the band structures of the top-cleaved plane parallel to the van der Waals spacing, and found Dirac-type topological surface states TSS2 between the α and β bands along the T-Y direction [Figs. 3(a), 3(b), and 3(d)]. The TSS2 in the bulk gap connect the parts of the α and β band originated from the Te p orbitals, which are just the projections of TSS1 in the side-cleaved plane mentioned above. We also performed ARPES measurements along the $\bar{Z}$-$\bar{\Gamma}$-$\bar{Z}$ direction with continuously changed photon energy to determine the high-symmetry points along the k_b direction in the bulk BZ, as exhibited in Fig. 3(c). Importantly, at the Fermi surface, two sets of bands labeled as SS and TSS2 remain unchanged when varying the photon energy, in strong contrast to the bulk bands at higher binding energy (see Fig. S5 [26]), further proving that they are both surface states.

One critical feature of topological surface states is spin-momentum-locked texture. To confirm the topological properties of $TaNiTe_5$ in its entirety, we measured the spin texture along the $\bar{Z}$-$\bar{\Gamma}$-$\bar{Z}$ direction on the top cleaved plane. The band structures detected in laser-ARPES [27] reveal two sets of surface states including TSS2, as clearly visualized in Fig. 3(e). Meanwhile, all features of the bulk and surface states are in excellent agreement with our calculations [Fig. 3(d)]. The spin texture was then measured

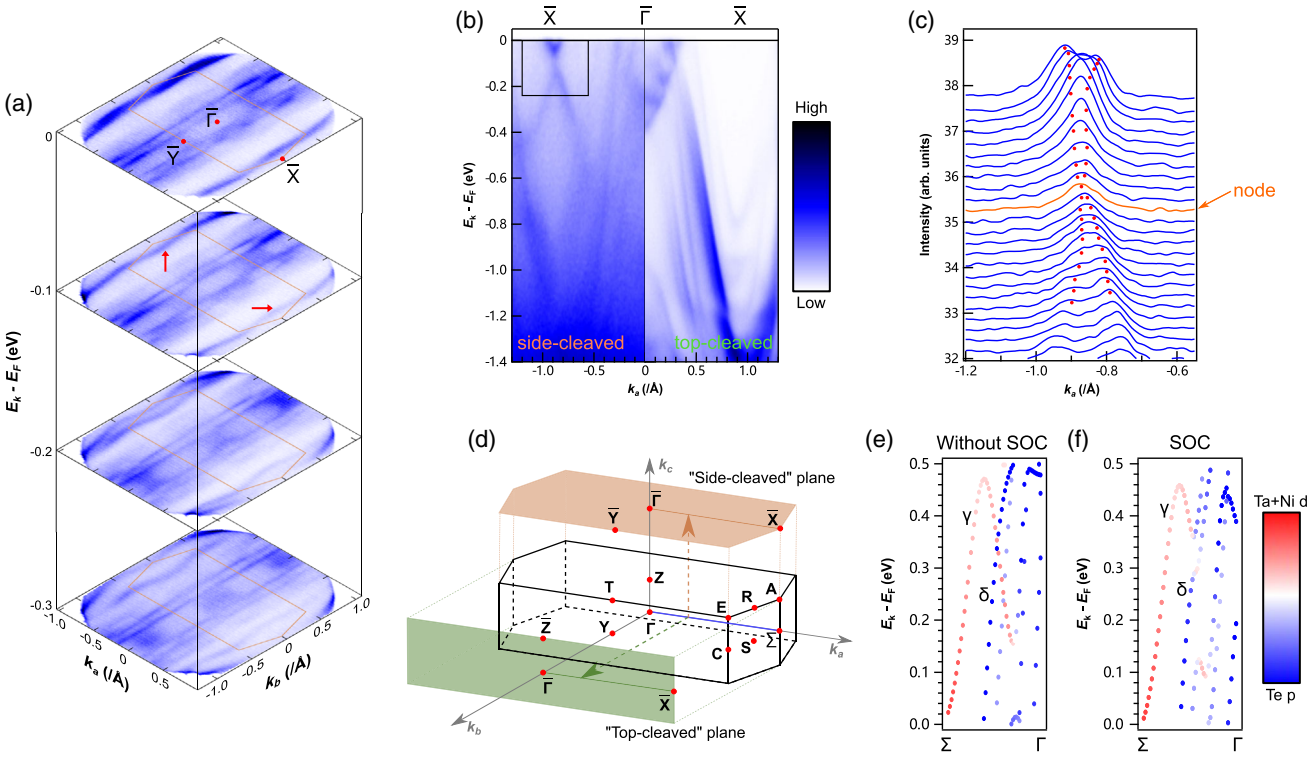

FIG. 4. Dirac-node arcs on side-cleaved plane: (a) Constant energy contour at different binding energy obtained at the side-cleaved plane by ARPES measurements ($h\nu = 70$ eV, red arrows indicate the Dirac-node arcs). (b) Experimentally measured band structures along the $\bar{X}$-$\bar{\Gamma}$-$\bar{X}$ direction on the side-cleaved plane (left, $h\nu = 65$ eV) and the top-cleaved plane (right, $h\nu = 86$ eV), respectively. (c) Magnified momentum distribution curves of the area indicated by the black rectangle in (b). The shape of the Dirac cone is fitted by red dots and the curve where the intersection lies is colored in orange. (d) The same Γ-Σ direction projected onto different cleaved surfaces. (e),(f) Calculated bulk bands along the Γ-Σ direction without and with SOC.

by laser-based SARPES [27]. Since the measured spin directions are perpendicular to the k_c (electron momentum) direction (Fig. S6 [26]), the results clearly reveal the spin-momentum-locked texture of TSS2 [Fig. 3(g) and Fig. S7 [26]], being consistent with the calculated spin texture [Fig. 3(f)], which prove them indeed topological nontrivial states arising from the strong topological order. In addition, although there should be no spin polarizations in bulk states theoretically due to the protection by time and space reversal symmetry, nonzero spin polarizations were observed experimentally for the bulk states showing opposite spin polarization compared to TSS2. This could be explained by the so-called "spin-layer locking" effect arising from the dipole field, which makes the spin polarization of the bulk states detectable due to the surface sensitivity of photoemission experiments [28,29].

Weak topological order.—It is worth noting that other Dirac-type surface states are present on the boundary of the BZ in the side-cleaved surface as exhibited in Fig. 4. The Dirac-cone-shaped electronic states are clearly resolved near the $\bar{X}$ point [Fig. 4(b) left panel], and their intersections form arc-shape states at about 0.1 eV below the Fermi energy [Fig. 4(a)]. Because the shape of bulk states is independent of the cleaved surfaces and these Dirac-type states vanish on the top-cleaved plane along the same $\bar{\Gamma}$-$\bar{X}$ direction as compared in the left and right panels of Fig. 4(b) (also see Fig. S8 [26]), the Dirac-type states on the side-cleaved plane with no k_z dispersion [Fig. S9 [26]] can safely be concluded to be surface states, indicating they constitute Dirac-node arcs [30].

Unfortunately, these novel Dirac-node arcs cannot be well reproduced in calculations. Such kind of discrepancy has also been reported in other systems, where the Dirac-node arcs have been observed experimentally [31,32]. These Dirac-type surface states that only emerge on a specific surface (side-cleaved pane) are the main feature of weak topological materials. Using the Wilson loop method [5,25,33–35], we calculated the Z_2 topological number $(v_0; v_1, v_2, v_3)$ for the δ band to identify the topological properties [here, v_0 is the strong topological index and (v_1, v_2, v_3) are the weak topological indices]. The resultant Z_2 index of the δ band is (0;001) as shown in Fig. S11 [26], verifying a weak topological phase.

In addition, band analysis parallel to the k_a direction, which possesses the lowest resistivity reported by the previous study [13], shows the presence of band inversion between γ and δ along the Γ-Σ direction [Figs. 4(e) and 4(f)]. This evidence suggests that Dirac-node arcs are formed by

the weak topological phase of $TaNiTe_5$ and proposes a possible reason for the highly anisotropic transport behaviors [13] in spectroscopy.

In summary, the quasi-1D material $TaNiTe_5$ was determined to be a strong topological material due to the band inversion between Ta and Ni d orbitals and Te p orbitals, which subsequently results in the topological surface states at both the side- and top-cleaved planes. With laser-based SARPES, a spin-momentum-locked texture for the surface states was clearly resolved, supporting the topologically nontrivial nature of these electronic states. Furthermore, the ARPES observation of Dirac-node arcs suggested a weak topological phase coexisting with the strong topological phase, demonstrating the $TaXTe_5$ family as a promising platform to investigate multiple topological phases coexisting in one material. Moreover, since such Dirac-node arcs originated from the weak topological order are located in the vicinity of the Fermi energy, $TaNiTe_5$ provides a practical platform to develop spintronics devices with high tunability by bias voltage methods.

This work was supported by the National Key R&D Program of China (Grant No. 2017YFA0305400). This work was also supported by JSPS KAKENHI, Japan (Grants No. JP19H00651, No. JP19H02683, No. JP21H04439, No. JP21H04652, No. JP22H04483 and No. JP22H01943), by MEXT Q-LEAP (Grant No. JPMXS0118068681), and by MEXT as "Program for Promoting Researches on the Supercomputer Fugaku" (Basic Science for Emergence and Functionality in Quantum Matter Innovative Strongly-Correlated Electron Science by Integration of "Fugaku" and Frontier Experiments, JPMXP1020200104) (Project ID: hp200132/hp210163/hp220166). The ARPES experiments were performed at BL03U of Shanghai Synchrotron Radiation Facility under the approval of the Proposal Assessing Committee of SiP.ME^2 platform project supported by the National Natural Science Foundation of China (Proposal No. 11227902, No. U1632266, No. 11927807 and No. U2032207). The laser-based SARPES measurements were conducted with the approval of the joint-research project of Synchrotron Radiation Laboratory in the Institute for Solid State Physics, The University of Tokyo, Japan. A. E. acknowledges funding by the Fonds zur Förderung der wissenschaftlichen Forschung (FWF) Grant No. I 5384. Calculations were performed at Rechenzentrum Garching of the Max Planck Society (Germany).

*Present address: Graduate School of Advanced Science and Engineering, Hiroshima University, Higashi-Hiroshima 739-8526, Japan.
†kondo1215@issp.u-tokyo.ac.jp
‡qiaoshan@mail.sim.ac.cn
‖yemao@mail.sim.ac.cn

[1] M. Z. Hasan and C. L. Kane, Rev. Mod. Phys. **82**, 3045 (2010).
[2] X.-L. Qi and S.-C. Zhang, Rev. Mod. Phys. **83**, 1057 (2011).
[3] A. Stern and N. H. Lindner, Science **339**, 1179 (2013).
[4] C.-Z. Chang *et al.*, Science **340**, 167 (2013).
[5] L. Fu, C. L. Kane, and E. J. Mele, Phys. Rev. Lett. **98**, 106803 (2007).
[6] L. Fu, Phys. Rev. Lett. **106**, 106802 (2011).
[7] W. A. Benalcazar, B. A. Bernevig, and T. L. Hughes, Science **357**, 61 (2017).
[8] B. Sbierski, M. Schneider, and P. W. Brouwer, Phys. Rev. B **93**, 161105(R) (2016).
[9] I. P. Rusinov, T. V. Menshchikova, A. Isaeva, S. V. Eremeev, Yu. M. Koroteev, M. G. Vergniory, P. M. Echenique, and E. V. Chulkov, Sci. Rep. **6**, 20734 (2016).
[10] N. Avraham *et al.*, Nat. Mater. **19**, 610 (2020).
[11] R. Noguchi *et al.*, Nature (London) **566**, 518 (2019).
[12] R. Noguchi *et al.*, Nat. Mater. **20**, 473 (2021).
[13] C. Xu *et al.*, J. Phys. Chem. Lett. **11**, 7782 (2020).
[14] W. Jiao *et al.*, Phys. Rev. B **102**, 075141 (2020).
[15] W. Jiao *et al.*, Phys. Rev. B **103**, 125150 (2021).
[16] Y. Li, Z. Ran, C. Huang, G. Wang, P. Shen *et al.*, Phys. Rev. Lett. **128**, 106802 (2022).
[17] Z. Hao, W. Chen, Y. Wang, J. Li, X.-M. Ma *et al.*, Phys. Rev. B **104**, 115158 (2021).
[18] S. Xiao *et al.*, Phys. Rev. B **105**, 195145 (2022).
[19] G. Kresse and J. Hafner, Phys. Rev. B **47**, 558(R) (1993).
[20] G. Kresse and J. Furthmüller, Phys. Rev. B **54**, 11169 (1996).
[21] G. Kresse and D. Joubert, Phys. Rev. B **59**, 1758 (1999).
[22] Z. P. Sun, Z. H. Liu, Z. T. Liu, W. L. Liu, F. Y. Zhang, D. W. Shen, M. Ye, and S. Qiao, J. Synchrotron Radiat. **27**, 1388 (2020).
[23] Y. Yang *et al.*, Nucl. Sci. Tech. **32**, 31 (2021).
[24] A. A. Mostofi, J. R. Yates, Y. Lee, I. Souza, D. Vanderbilt, and N. Marzari, Comput. Phys. Commun. **178**, 685 (2008).
[25] Q. S. Wu, S. N. Zhang, H. F. Song, M. Troyer, and A. A. Soluyanov, Comput. Phys. Commun. **224**, 405 (2018).
[26] See Supplemental Material at http://link.aps.org/supplemental/10.1103/PhysRevLett.129.146401 for additional information concerning the 1. Characterization of $TaNiTe_5$ single crystals; 2. Termination of the side-cleaved surface; 3. Verification of strong topological surface states; 4. High symmetry points on the top-cleaved plane; 5. Laser-based SARPES measurements; 6. Verification of weak topological surface states; 7. Z_2 topological invariants.
[27] K. Yaji *et al.*, Rev. Sci. Instrum. **87**, 053111 (2016).
[28] X. Zhang, Q. Liu, J. Luo, A. J. Freeman, and A. Zunger, Nat. Phys. **10**, 387 (2014).
[29] K. Gotlieb, C.-Y. Lin, M. Serbyn, W. Zhang, C. L. Smallwood, C. Jozwiak, H. Eisaki, Z. Hussain, A. Vishwanath, and A. Lanzara, Science **362**, 1271 (2018).
[30] Y. Wu, L.-L. Wang, E. Mun, D. D. Johnson, D. Mou, L. Huang, Y. Lee, S. L. Bud'ko, P. C. Canfield, and A. Kaminski, Nat. Phys. **12**, 667 (2016).
[31] D. Takane, Z. Wang, S. Souma, K. Nakayama, C. X. Trang, T. Sato, T. Takahashi, and Y. Ando, Phys. Rev. B **94**, 121108 (R) (2016).
[32] T. Nakamura *et al.*, Phys. Rev. B **99**, 245105 (2019).
[33] L. Fu and C. L. Kane, Phys. Rev. B **76**, 045302 (2007).
[34] A. A. Soluyanov and D. Vanderbilt, Phys. Rev. B **83**, 235401 (2011).
[35] H. Weng, X. Dai, and Z. Fang, MRS Bull. **39**, 849 (2014).